Molecular Line Profiles from a Core Forming in a Turbulent Cloud

Jeong-Eun Lee

Department of Astronomy and Space Science, Astrophysical Research Center for the Structure and Evolution of the Cosmos, Sejong University, 98 Gunja-Dong, Gwangjin-Gu, Seoul 143-747, Korea

jelee@sejong.ac.kr

and

Jongsoo Kim

Korea Astronomy and Space Science Institute, Hwaam-Dong, Yuseong-Gu, Daejeon 305-348, South Korea

jskim@kasi.re.kr

ABSTRACT

We calculate the evolution of molecular line profiles of HCO^+ and $C^{18}O$ toward a dense core that is forming inside a magnetized turbulent molecular cloud. Features of the profiles can be affected more significantly by coupled velocity and abundance structures in the outer region than those in the inner dense part of the core. The velocity structure at large radii is dominated by a turbulent flow nearby and accretion shocks onto the core, which resulting in the variation between inward and outward motions during the evolution of the core. The chemical abundance structure is significantly affected by the depletion of molecules in the central region with high density and low temperature. During the evolution of the core, the asymmetry of line profiles easily changes from blue to red, and vice versa. According to our study, the observed reversed (red) asymmetry toward some starless cores could be interpreted as an intrinsic result of outward motion in the outer region of a dense core, which is embedded in a turbulent environment and still grows in density at the center.

Subject headings: astrochemistry — ISM: molecules — ISM: clouds — stars: formation — MHD — methods: numerical

1. Introduction

Stars form inside very dense molecular clouds by gravitational collapse. Starless dense cores, which have been considered as potential sites of future star formation, have been used to study the initial conditions of star formation. There is, however, no straightforward method to determine whether specific cores will actually form stars. Observations tell us the mass or density profile of a core, which provides clues to whether the core is gravitationally bound or unstable to collapse to form a star in the future.

Walker et al. (1986) and Zhou et al. (1993) interpreted the asymmetry of line profiles with blue stronger peaks (*blue asymmetry*), which have been seen in optically thick self-absorbed lines, as an infall signature. Gregersen & Evans (2000) and Lee et al. (2001) have surveyed dense starless cores with molecular lines of HCO^+ 3−2 and CS 2−1. The infall signature is seen in about 35% and 50% of the observed starless cores of each survey, respectively. The infall signature, however, occurs in much larger scales across the face of a core opposed to the collapsing center expected from the inside-out collapse model (Shu 1977), indicative of an overall inward motion.

This overall inward motion in starless dense cores could be considered as a result of a supercritical (or slightly subcritical) ambipolar diffusion model in Ciolek & Basu (2000). The inward velocity profile in L1544, the canonical starless dense core, is able to be reproduced reasonably well with the model (Caselli et al. 2002). However, in addition to the blue asymmetry, the *reversed asymmetry*, which has a red stronger peak in the self-absorption feature, is also seen toward many starless cores. This reversed asymmetry cannot be caused by outflows, which can be developed only after an accretion disk forms around a young stellar object. However, by definition, a starless core can not harbor the young stellar object. Other studies claim that the reversed asymmetry might be caused by rotation (Redman et al. 2004; Lee et al. 2007) or oscillation (Keto et al. 2006; Maret et al. 2007; Aguti et al. 2007) of dense cores.

As described above, the interpretation of the velocity profiles toward starless dense cores is still controversial since the formation process of dense cores is not well understood. Here, we suggest a possible explanation of the reversed red asymmetry observed toward some starless cores with the theory based on turbulence since it involves not only inward but also outward motions in a core formed from the density fluctuations of a larger turbulent cloud (see, e.g., Mac Low & Kessen 2004). In addition to the dynamical process, the chemical process in a dense core can also affect molecular line profiles (Rawlings & Yates 2001, Lee et al. 2003, 2004, 2005). Therefore, observed line profiles must be interpreted based on both the dynamics and chemistry of a core.

In this Letter, we combine dynamics and chemistry in order to study the evolution of molecular line profiles toward a dense core forming within a large turbulent cloud. We show that the velocity structure at the outer part of the core can significantly affect molecular line profiles. Indeed, simulated line profiles exhibit a mixture of infall and outflow signatures as a function of time. Thus a snap shot of core conditions of a single object cannot provide a full accounting of core formation and evolution toward collapse. This Letter is organized as follow. The dynamical and chemical models of a core are presented in §2, results, and summary and discussion are given in §3 and §4, respectively.

2. Dynamical and Chemical models of a Core

2.1. Dynamical Evolution of a Core

What we are interested in this study is to follow up the evolution of molecular line profiles of a core forming in a turbulent molecular cloud. For this purpose, we perform a couple of three-dimensional numerical experiments of a self-gravitating, isothermal, turbulent, magnetized molecular cloud. In fact, we integrate, as a function of time, the isothermal MHD and Poisson equations. The number of cells used in the experiments is 512^3. A typical core is covered with more than 32^3 cells.

There are two parameters in the numerical experiments: one is the plasma β, which is the ratio of gas pressure to magnetic pressure, and the other is the Jeans number J, which is the ratio of the one dimensional size of a computational box L, to the Jeans length L_J. A mass-to-flux ratio normalized with its critical value μ, can be written in terms of these two parameters $\mu = \pi J\sqrt{\beta/2}$, where we use the critical mass-to-flux ratio $(M/\phi)_{\rm cr} = (4\pi^2 G)^{-1/2}$ in Nagano & Nagamura (1978). Initially a uniform molecular cloud is threaded with a uniform magnetic field. In order to generate a turbulent flow and keep the level of the turbulence inside the molecular cloud, we add velocity perturbations generated in the Fourier space with wavelengths that span from half to full size of the box. We adjust the input rate of the kinetic energy so that the root-mean-square sonic Mach number M_s of a turbulent flow becomes 10 (Mac Low 1999; Stone et al. 1998). Once a fully saturated turbulent flow is generated, we turn on the self-gravity of gas and follow up the evolution of a densest core formed in the cloud. If $\beta = 0.1$ and $J = 4$, then the μ value is 2.8. So the initial molecular cloud is in a highly supersonic ($M_s >> 1$), Jeans unstable ($J > 1$), and magnetically supercritical ($\mu > 1$) state.

Since the combined isothermal MHD and Poisson equations can be written in dimensionless form with the two parameters, we can select any units of, for example, length, time,

and mass in such a way that they are scalable with each other. However there is one more additional parameter M_s, which is used to fix these units. If Larson's relation between the sizes and velocity dispersions of clouds (Larson 1981) holds for our model cloud, then the Mach number, which is the velocity dispersion of our model cloud, can determine its corresponding size. In fact, a Larson-type relation of the form $M_s = 5(L/1\mathrm{pc})^{1/2}$, if we take 0.5 as the power index (for example, Myers 1983), is used. Then density and magnetic field strength could be determined from relations, $n = 500(J/(L/1\mathrm{pc}))^2$ cm^{-3}, and $B = 0.205(n/\beta)^{1/2}$ μG (see also equation (7) and equation (8) in Vázquez-Semadeni et al. 2005). So if we choose $\beta = 0.1$, $J = 4$, and $M_s = 10$, the size of our computational box, the initial number density, and the initial magnetic field strength become 4 pc, 500 cm^{-3}, and 14.5 μG, respectively.

Our dynamical model has a few limitations such as turning on self-gravity after generating a fully saturated turbulent flow, driving turbulent flows by adding velocity fields generated in the Fourier space, not taking into account ambipolar diffusion, and assuming the isothermal condition. However, they are common in numerical models of a turbulent molecular cloud (see, for example, Klessen et al. 2000; Ostriker et al. 2001; Li et al. 2004; Vazquez-Semadeni et al. 2005). Due to the limited space, we only mention the effects of the latter two limitations on our results. If ambipolar diffusion is included in our model, then the ambipolar diffusion process is more important in the central part of a core where the degree of ionization is lower than that of the outer part of the core. Since our synthesized line profiles are more sensitive to the conditions at the outer layer (see section 3), our main results are not likely to be significantly affected by ambipolar diffusion. We also take the isothermal approximation which enables us not to solve the energy equation with cooling and heating processes. To take into account the cooling and heating processes of gas realistically entails a heavy calculation because molecular cooling lines are usually optically thick. When line profiles are, however, synthesized, we calculate two cases with a constant temperature and temperature variations of gas and dust inside the core (see section 3). We present the latter case only because the line features from both cases are not much different from each other.

2.2. Chemical Evolution and the HCO^+ Line Evolution

In order to calculate the chemical evolution in the core picked-up from the dynamical simulation as described in the previous subsection, we adopt the evolutionary chemical model developed by Lee et al. (2004), in particular, the model before collapse begins. In the prestellar phase where this paper focuses on, the model calculates the chemical evolution at each grid point as density grows with time. The chemical network in the model has been

updated to include more recent results on the binding energy of N_2 (Öberg et al. 2005) and the photodesorption yield of CO (Öberg et al. 2007). For the initial molecular abundances of the coupled evolution between dynamics and chemistry, we calculate the chemical evolution in a constant density of 5×10^3 cm^{-3} with the same initial atomic abundances as used in Lee et al. (2004) for $t = 5 \times 10^5$ years. For the chemical calculation, the dense core is assumed to be surrounded with material of $A_V = 1.0$ mag, where CO is self-shielded. For consistency, adopting the methods used in Lee et al. (2004), we also calculate the dust and gas temperatures with the interstellar radiation field attenuated by $A_V = 1.0$ mag. The time step for data dump of the dynamical simulation is 4×10^4 years, during which the chemistry is calculated based on constant density and temperatures given at a specific dump time, and the result of the chemical evolution is used as initial conditions for the next dump time.

We use the Monte-Carlo method (Choi et al. 1995) to perform the radiative transfer calculation for the HCO^+ and $C^{18}O$ lines. The collision rates for HCO^+ and CO are adopted from Flower (1999) and Flower & Launay (1985). For the simulation of the line profiles, we assume the distance to the model core of 250 pc and the beam sizes for the Caltech Submillimeter Observatory 10.4 m telescope. We also include a constant microturbulent velocity dispersion of 0.2 km s^{-1}. We model the HCO^+ 3−2 and 4−3 transitions, which have been used to study infall motion in low mass cores with and without young stellar objects (Gregersen et al. 1997; Gregersen & Evans 2000). The optically thin $C^{18}O$ 3−2 line is also modeled to be compared to the HCO^+ line profiles.

3. Results

We use a one-dimensional (radial) chemical network coupled with a radiative transfer model to simulate line profiles. For this purpose we have to reduce the three-dimensional density and velocity fields into one-dimensional radial distributions using the following procedures. First, we find the position of a density peak of the whole computational domain, which is taken as the origin of the radial coordinate. Second, we identify a core as a connected region whose density is larger than $n_{H_2} = 10^3$ cm^{-3}. Third, we subtract a center-of-mass velocity of the core from its velocity field. The three-dimensional center-of-velocity of the core ranges from 0.2 km sec^{-1} to 2.0 km sec^{-1} Fourth, we take the average of the density and radial velocity at each spherical shell with the width of a computational cell. At this point we have to mention the effect of the radial averaging that we have taken in the above. The averaging certainly smoothed out density and velocity variations at an outer layer affected by, for example, a shock. So the line profiles observed towards a specific direction may show much stronger variation than the line profiles that are obtained after taking the

radial averaging.

In Figure 1, we plot the density and velocity profiles as a function of the radial distance from the center of the core. The two digit numbers are the elapsed time in units of 40,000 years after turning on self-gravity. We can clearly see from density profiles that the central density of the core is increasing as time goes on. The power index of density profiles in the outer region is increasing from shallower than -2 at an earlier time to steeper than -2 at a later time. At a given radial distance, the density and velocity dispersions are much smaller than the radially averaged density and velocity, respectively.

The radial velocity profiles are quite interesting. In the central part of the core, most of the profiles have negative but very small velocity, which means that the central part of core is slowly collapsing. In the outer part of the core, the profiles have both positive and negative signs and their amplitudes are larger than the thermal sound speed. The large-amplitude velocity profiles are due to not only the large-scale turbulent flow nearby the core but also accretion shocks onto the core. Even though we do not show radial density and velocity profiles from a simulation with a weak initial field strength, $\beta = 1.0$, the large-amplitude velocity profiles in the outer part of a core are also found. However, infall velocities in the central part of the core have a bit larger (but still have a subsonic speed) than ones of the case with $\beta = 0.1$.

Figure 2 shows the comparison between dust and gas temperatures calculated based on the dust continuum radiative transfer and the balance between heating and cooling of gas, respectively. The gas temperature is decoupled from the dust temperature at densities $\leq 5 \times 10^4$ cm^{-3}, where gas-grain collisions is not dominant, and has peaks at the surface of the model core due to the photoelectric heating.

The evolution of the HCO^+ radial abundance calculated based on the density and temperature evolution is presented in Figure 3. As expected, at small radii, HCO^+ is significantly depleted from the gas phase as density grows because CO becomes frozen-out onto grain surfaces (Lee et al. 2003, 2004 and references therein) in such dense and cold conditions. The abundance drops at the core surface due to the dissociative recombination of HCO^+ with electrons. As described in §2.2, the chemical evolution is calculated at each grid point without following each gas parcel (that is, assuming the quasi-static evolution) due to the following reasons. In the inner region of the core, the static evolution is a good approximation since the velocity is much smaller than the sound speed. In the outer part of the core, however, densities are low, and thus the chemical time scale is too long to be affected by the movement of gas parcels. For example, an infalling gas parcel with the infall velocity of 0.5 km s^{-1} at the surface moves inward only $\sim$0.02 pc for 40,000 years, and the densities of two positions are not very different. This assumption is also well supported in

Figure 3. The abundance of HCO^+ varies significantly at small radii, but at radii greater than 0.1 pc, where velocities are possibly greater than the sound speed, the abundance does not vary much with time.

Figure 4 presents the evolution of the HCO^+ 3−2, 4−3, and $C^{18}O$ 3−2 line profiles toward the core center. The two digit number in each panel represents the elapse time in units of 40,000 years after turning on the self-gravity. The first upper left panel shows line profiles at 1×10^6 $(25 \times 40,000)$ years and the time of the second panel is increased by 8×10^4 $(2 \times 40,000)$ years from the first one, and so on. Although the density grows with time, the $C^{18}O$ 3−2 line becomes weaker since CO is depleted from gas due to its freeze-out onto grain surfaces. The most important trend seen in this study is that the asymmetry of the HCO^+ 3−2 line profile mostly depends on the velocity structure at the outer part of the core. In the comparison of line profiles with the velocity structures (Figure 1b), if the velocity at large radii shows infall motion(e.g., at the time of 37), the HCO^+ line has the infall asymmetry with a blue stronger peak. On the other hand, the line profile represents the reversed asymmetry with a red stronger peak when the velocity at large radii shows outward motion (e.g., at the times of 25, 31, and 49). This result is caused by the combination of the abundance and velocity profiles; HCO^+ is depleted at small radii so that the HCO^+ 3−2 lines effectively form at rather large radii in the core, where velocities are dominated by the turbulent flow and accretion shocks. The kinetic temperature also increases outward. As a result, the excitation temperature of HCO^+ 3−2 peaks around 0.1 pc. Even the broad line feature seen at time 43, which may be interpreted as an infall at the core center in actual observations, is caused by the motion at large radii of the core rather than that occurring at small radii.

In the comparison of the HCO^+ 4−3 line (gray) with the 3−2 line (black solid) in Figure 4, the 3−2 line shows the reversed asymmetry while the blue asymmetry appears in the HCO^+ 4−3 line at time 25 and 29 (the opposite feature at time 35 and 47) although the difference between blue and red peak strengths is not significant. This varying asymmetry in different transitions of a molecule has been observed (e.g., L1157 in Gregersen et al. 1997; B68 in Maret et al. 2007). In addition, the relative strength between two peaks of the HCO^+ 3−2 line is reduced in the 4−3 line at the times of 31 and 39. These trends are featured since the two transitions trace different radii of the core, for example, at time 25, the 4−3 line traces a deeper region, which has inward motion, while the 3−2 line traces the less dense outer region, which shows outward motion.

We assume that our model core of a radius 0.25 pc is at a distance 250 pc. Its angular size is about $200''$. Since physical conditions of the core at around 0.1 pc ($\sim 80''$) mainly contribute to the line formation, a telescope beam size that is not larger than the angular

size of the core does not significantly affect the line intensity and shape shown in Figure 4.

4. Summary and Discussion

We traced, through a high-resolution numerical experiment, the evolution of a core forming in a turbulent molecular cloud that is in a Jeans unstable and magnetically supercritical state. The core is slowly contracting at the central part with a subthermal speed. Due to the influence of accretion shocks and a nearby turbulent flow, velocity fields in the outer region of the core can easily exceed the thermal speed, and show not only the contracting but also sometimes expanding motions. Based on the evolutionary profiles of density and gas and dust temperatures, we calculated the evolution of the HCO^+ abundance. Once the central density of the core is larger than 10^5 cm^{-3}, the HCO^+ abundance profiles peak at outer regions because of the depletion of HCO^+ at the central part of the core (see Figure 3). We also calculated the evolution of HCO^+ 3−2, 4−3, and $C^{18}O$ 3−2 line profiles that are coupled to the density, kinetic temperature, and abundance structures. The most interesting result in this work is that the HCO^+ line profiles are dominantly affected by the velocity profiles at the outer regions. This is the consequence of both the HCO^+ abundance and velocity profiles that have peaks at the outer regions.

We showed that the molecular line profiles of a core, which results from the coupled velocity and chemical structures, vary with time. To understand the formation process of cores, survey observations of many cores in different evolutionary states are crucial. Mapping observations of individual cores with a high resolution enables us to know the complex velocity structures of the cores. The radial variation of the velocity field as seen in B68 may be an intrinsic part of star formation, and the blue asymmetry is not always a direct signature of collapse in starless dense cores (Keto et al. 2006).

We are very grateful to Ted Bergin for valuable comments. This work was supported by the Korea Science and Engineering Foundation under a cooperative agreement with the Astrophysical Research Canter for the Structure and Evolution of the Cosmos.

REFERENCES

Aguti, E.D., Lada, C.J., Bergin, E.A., Alves, J.F., & Birkinshaw, M. 2007, ApJ, 665, 457

Caselli, P., Walmsley, C. M., Zucconi, A., Tafalla, M., Dore, L., & Myers, P. C. 2002, ApJ, 564, 331

Choi, M., Evans, N. J., II, Gregersen, E. M., & Wang, Y. 1995, ApJ, 448, 742

Ciolek, G. E., & Basu, S. 2000, ApJ, 529, 925

Flower, D.R., & Launay, J.M, 1985, MNRAS, 214, 271

Flower, D.R. 1999, MNRAS, 305, 651

Gregersen, E.M., Evans, N.J.II., Zhou, S., & Choi, M., 1997, ApJ, 484, 256

Gregersen, E.M., & Evans, N.J.II 2000, ApJ, 538, 260

Keto, E., Broderick, A.E., Lada, C.J., & Narayan, Ramesh 2006, ApJ, 652, 1366

Klessen R. S. 2000, ApJS, 535, 869

Larson, R.B. 1981, MNRAS, 194, 809

Lee, C.W., Myers, P.C., & Tafalla, M. 2001, ApJS, 136, 703

Lee, J.-E., Evans, N.J.,II, Shirley, Y.L., & Tatematsu, K. 2003, ApJ, 583, 789

Lee, J.-E., Bergin, E.A., & Evans, N.J.II 2004, ApJ, 617, 360

Lee, J.-E., Evans, N.J.II, & Bergin, E.A. 2005, ApJ, 631, 351

Lee, J.-E., Di Francesco, J., Bourke, T.L., Evans, N.J.II, Wu, J. 2007, ApJ, 671, 1748

Li, P. S., Norman, M. L., Mac Low, M.-M., & Heitsch, F. 2004, ApJ, 605, 800

Nakano, T. & Nakamura, T. 1978, PASJ, 30, 671

Mac Low, M.-M. 1999, ApJ, 524, 169

Mac Low, M.-M., & Klessen, R. S. 2004, Rev. Mod. Phys., 76, 125

Maret, S., Bergin, E.A., & Lada, C.J. 2007, ApJ, 670, 25

Myers, P. C. 1983, ApJ, 270, 105

Öberg K.I., van Broekhuizen, F., Fraser, H. J., Bisschop, S. E., van Dishoeck, E. F., & Schlemmer, S. 2005, ApJ, 621, 33

Öberg K.I., Fuchs, G.W., Awad, Z., Fraser, H.J., Schlemmer, S., van Dishoeck, E.F., & Linnartz, H. 2007, ApJL, 662, 23

Ostriker, E. C., Stone, J. M., & Gammie, C. F. 2001, ApJ, 546, 980

Rawlings, J.M.C., & Yates, J.A. 2001, MNRAS, 326, 1423

Redman, M.P., Keto, E., Rawlings, J.M.C., & Williams, D.A. 2004, MNRAS, 352, 1365

Shu, F.H. 1977, ApJ, 214, 488

Stone, J. M., Ostriker, E. C., & Gammie, C. F. 1998, ApJ, 508, L99

Vázquez-Semadeni, E., Kim, J., Shadmehri, M., Ballesteros-Paredes, J. 2005, ApJ, 618, 344

Walker, C. K., Lada, C. J., Young, E. T., Maloney, P. R., & Wilking, B. A., 1986, ApJ, 309, L47

Zhou, S., Evans, N.J.II, Koempe, C., & Walmsley, C.M. 1993, ApJ, 404, 232

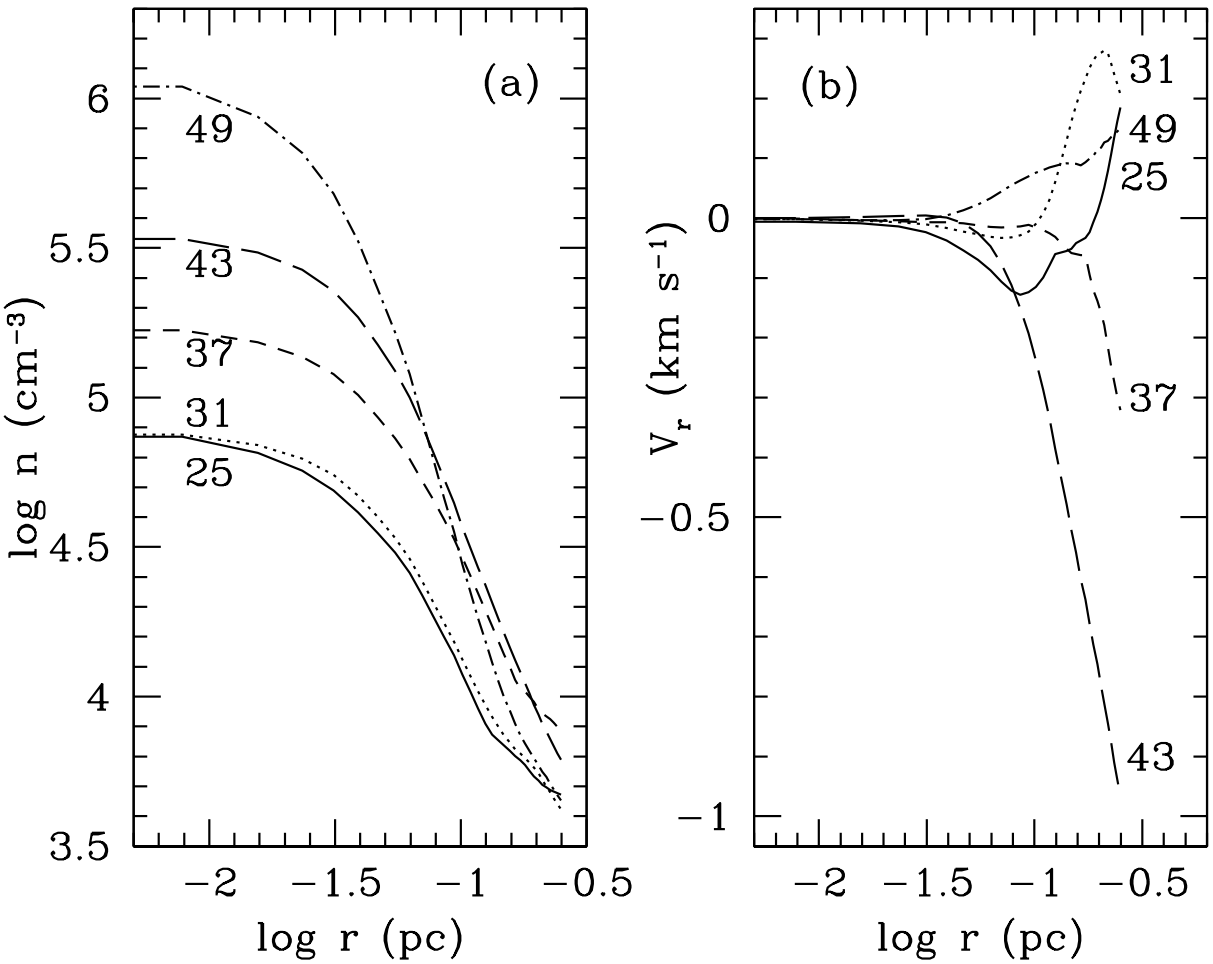

Fig. 1.— The evolution of density and velocity profiles. Two digit numbers represent time in units of 40,000 years.

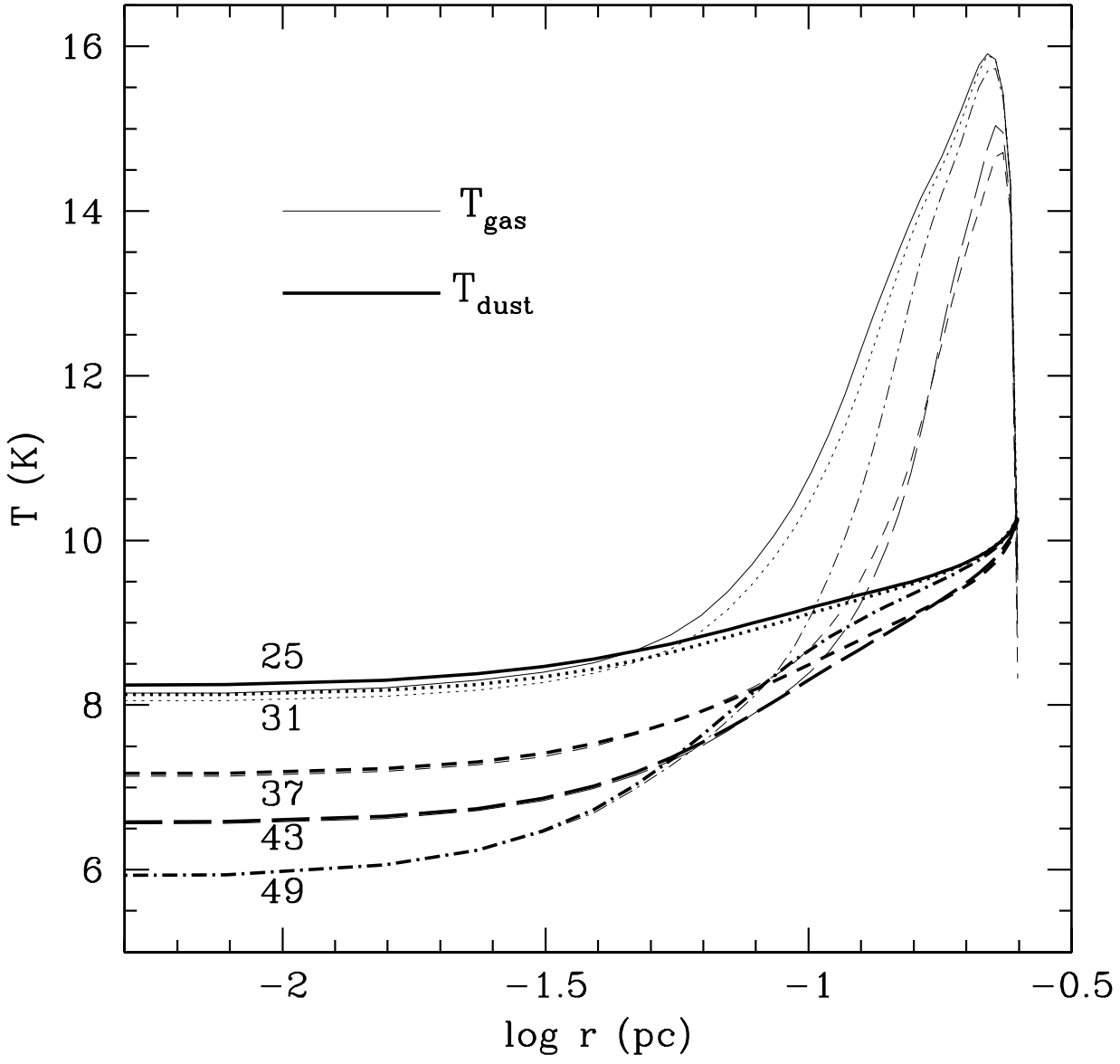

Fig. 2.— The evolution of the gas (thin lines) and dust (thick lines) temperature profiles. The two digit numbers represent time in units of 40,000 years.

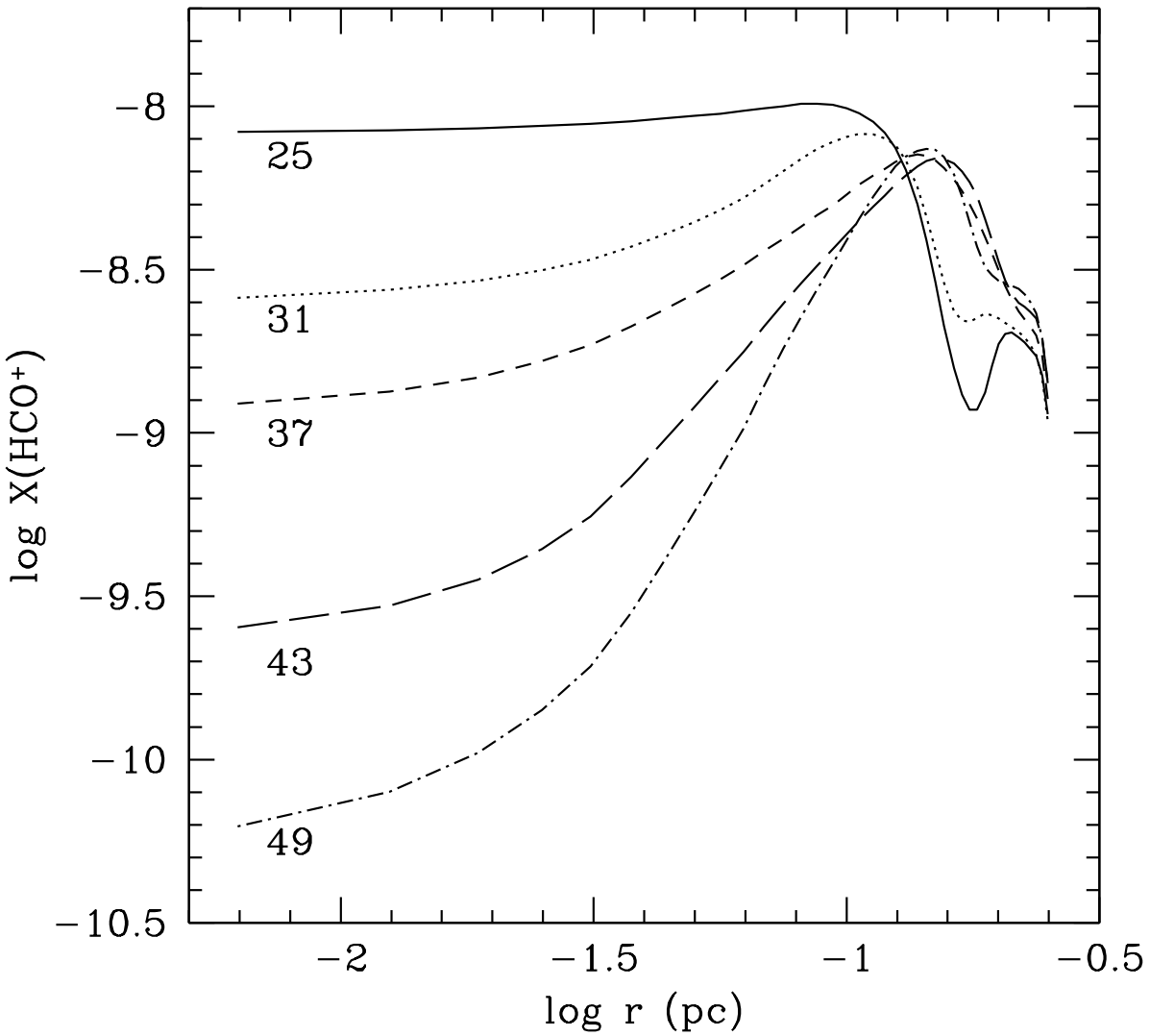

Fig. 3.— The evolution of the HCO^+ abundance profiles. The two digit numbers represent time in units of 40,000 years.

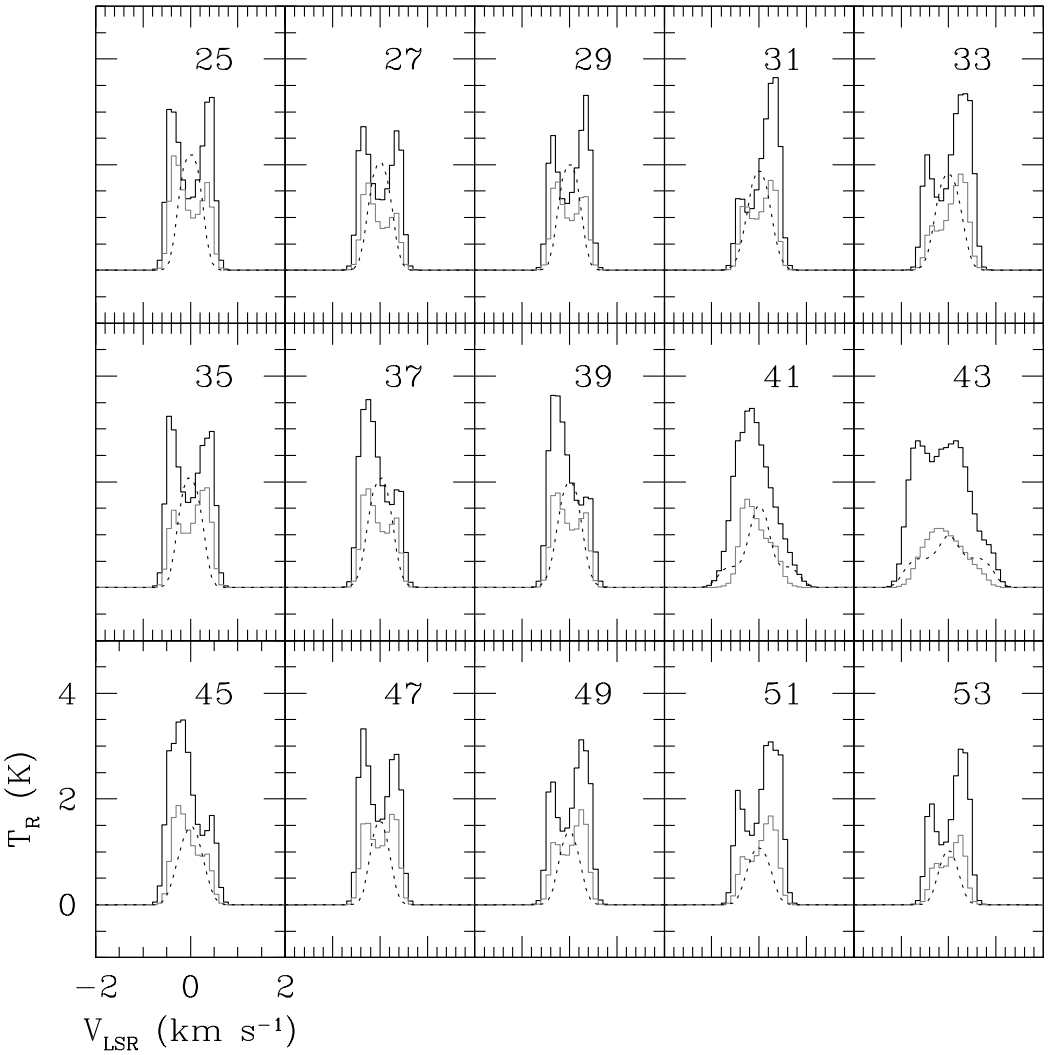

Fig. 4.— The evolution of molecular line profiles. The black and gray solid histograms represent the HCO^+ 3−2 and 4−3 line profiles, respectively. The dotted lines show the $C^{18}O$ 3−2 lines. The beam sizes are 26″ for HCO^+ 3−2 and $C^{18}O$ 3−2 and 20″ for HCO^+ 4−3, respectively. The angular size of our model core with a radius of 0.25 pc at a distance of 250 pc is around 200″ . The two digit numbers represent time in units of 40,000 years.